Maneuver Optimization of Aircraft Utilizing High Angles of Attack

K. H. Well
Research Scientist, DFVLR Oberpfaffenhofen

B. Faber
Research Engineer, MBB Ottobrunn

E. Berger
Program Analyst, DFVLR Oberpfaffenhofen

Abstract

Future high performance aircraft will have high thrust/weight ratios, will be equipped with CCV technology, will be extremely light weight, and possibly have the capability of flying at very high angles of attack - in the "Poststall" (PST) region. This paper investigates by using numerical optimization techniques whether the PST-capability improves performance for several tactical maneuvers. Specifically minimum time turning maneuvers for a variety of boundary conditions and flight path constaints are computed i) for aircraft A which has PST-capability ii) for aircraft B which does not but is otherwise identical with A. It is concluded that for two combinations of boundary conditions/path constraints flight time can be reduced if high angles of attack are utilized. In the majority of cases, however, minimum time maneuvers are flown - load constraints permitting - at or near C_{Lmax}.

List of Symbols

a	velocity of sound/coefficient of polynomial
b	coefficient of polynomial
B	approximation to Hesse matrix
c	coefficient of polynomial
C_D	drag coefficient
C_L	lift coefficient
C_T	thrust coefficient
$C_{\dot{m}}$	specific fuel consumption coefficient
C_{LP_α}	slope of lift coefficient vs α of pursuer
D	aerodynamic drag force
d	distance between pursuer and evader
g	acceleration of gravity/vector of constraint functions
h	altitude
H	variational Hamiltonian
L	Lagrangian function/lift force
m	aircraft mass/number of control function
M	Machnumber
n	number of state variables
N	resulting force normal to flight path
nzcl	number of coefficients of numerator polynomial for $C_L(\alpha)$
nzcd	number of coefficients of numerator polynomial for $C_D(\alpha)$
nncl	number of coefficients of denumerator polynomial for $C_L(\alpha)$
nncd	number of coefficients of denumerator polynomial for $C_D(\alpha)$
ncth	number of coefficients of polynomial in h for C_T
nctm	number of coefficients of polynomial in M for C_T
ncmh	number of coefficients of polynomial in h for $C_{\dot{m}}$
ncmm	number of coefficients of polynomial in M for $C_{\dot{m}}$
ncmd	number of coefficients of polynomial in δ for $C_{\dot{m}}$
n_z	load factor in direction of z-axis (body axes)
n_{za}	load factor normal to flight path
n_p	normed acceleration of pursuer
p	search direction
q	number of final conditions
S	reference area
T	resulting force tangential to flight path
T_T	thrust
T_p	thrust of pursuer
u	control vector of optimal control problem
V	aircraft true airspeed
V_k, V_l, V_m, V_n, V_t	velocity components (see Figure 3)
x	state vector of optimal control problem
x_g, y_g, z_g	geodetic coordinates
y	vector of decision variables
α	angle of attack
β	aspect angle
γ	flight path angle
δ	power setting
ζ, κ	auxiliary state variables
η_K	speed brake angle
ϑ_i	parameter in NLP algorithm
θ	pitch angle (body axes/geodatic axes)
λ, ν	Lagrange multipliers
μ	velocity bank angle
ϕ	bank angle (body axes/geodatic axes) /cost function
φ	vector of right hand sides
χ	velocity yaw angle
ρ	density of atmosphere
ψ	yaw angle (body axes/geodatic axes)
Ψ	vector of boundary conditions
ω_p	angular velocity of line of sight

Subscripts

ref	reference value
o,f	initial, final value
1,2,3	engine states
H	auxiliary variable
max,min	maximum, minimum values
P	pursuer

Introduction

A future tactical fighter aircraft with a delta wing and with thrust exceeding its weight may be capable of flying at very high angles of attack - in the "Poststall" (PST) mode. The analysts were asked if this capability will improve performance. It was decided to answer the question in two ways: i) by conducting air combat simulations in a manned simulator with two aircraft participating, aircraft A with PST-capability and aircraft B without. Advantages and disadvantages of the PST-capability were judged by the two participating pilots; ii) by using trajectory optimization methods with essentially identical physical data to those used in the manned simulations. Advantages and disadvantages of the PST-capability were obtained by comparing optimal trajectories of both aircraft for several typical flight maneuvers. While the first approach is more general as far as evaluating the overall performance is concerned the second approach is more methodical and provides precise numerical data about advantages and also clear interpretations.

This paper deals with the second approach only. It is a summary of ref. [1] and is divided into three parts. The first part contains a description of the point-mass equations for threedimensional flight, a presentation of typical aerodynamic data for a PST-aircraft, typical engine data, and the approximation of those data using rational function.

The second part gives a brief description of the numerical optimization method used, namely parameterization of the control functions of the optimal control problem and solution of the resulting nonlinear programming problem via multiplier methods.

In the third part several turning maneuvers with different boundary conditions are discussed. Since fast maneuvering is most important for air combat flight time was used as cost function in all cases. With given initial state first minimum time turning maneuvers (TM's) for i) free final state, ii) free final state except altitude prescribed, iii) fixed final state, iv) free final state with fuselage direction prescribed (fuselage pointing). Next, a slicing maneuver (SM) is computed. It consists of two sequential minimum time TM's in opposite direction with the additional constraint that the fuselage attitude should be positive at all times. This constraint guarantees certain visibility conditions for the pilot. Last, two optimal evasive maneuvers (EM's) are presented with two participating aircraft. Here, the objective was to find out if aircraft A can evade a pursuer flying strictly according to a pure pursuit guidance law. The first EM with the relative heading of both aircraft of 90°, the second EM with 0°. All numerical results will be discussed and summarized in the conclusion.

Equations of Motions

System Equations

The three dimensional motion of a point-mass vehicle over a flat, non rotating earth assuming no sideslip is described by the differential equations

$$\begin{aligned} m\dot{V} &= T-mg\sin\gamma \\ mV\dot{\chi} &= N\sin\mu/\cos\gamma \\ mV\dot{\gamma} &= N\cos\mu-mg\cos\gamma \\ \dot{x}_g &= V\cos\gamma\cos\chi \\ \dot{y}_g &= V\cos\gamma\sin\chi \\ -\dot{h} = \dot{z}_g &= -V\sin\gamma \\ \dot{m} &= -C_{\dot{m}}T_T \end{aligned} \qquad (1)$$

with

$$T = T_T\cos\alpha-D, \quad N = T_T\sin\alpha+L \quad . \qquad (2)$$

The aerodynamic and propulsive forces are determined by the following equations:

$$\begin{aligned} T_T &= C_T(h,M,\delta)T_{ref} \\ L &= C_L(\alpha,M)\rho(h)/2SV^2 \\ D &= C_D(\alpha,\eta_K,M)\rho(h)/2SV^2 \end{aligned} \qquad (3)$$

with the Machnumber $M=V/a(h)$. For given control-functions $\alpha(t),\mu(t),\delta(t),\eta_K(t)$ and for given initial state variables $V_o,\chi_o,\gamma_o,x_{go},y_{go},z_{go},m_o$ the system (1) can be integrated and has a unique solution.

Approximation of Data

The aerodynamic and propulsive coefficients C_L,C_D,C_T, $C_{\dot{m}}$ are functions of several variables and given as tables only. In order to apply any of the existing optimization algorithms these data must be approximated by sufficiently differentiable functions. For the sample aircraft the aerodynamic coefficients are given as

$$C_L(\alpha),\ C_D = C_{DO}(\alpha)+C_{DK}(\eta_K,M) \quad , \qquad (4)$$

where C_{DO} is the drag coefficient for $\eta_K=0$ and C_{DK} the additional one due to speed brakes $\eta_K\neq 0$. The thrust coefficient is given for three engine states, namely $C_{T1}(h,M)$ for "idle", $C_{T2}(h,M)$ for maximum "normal power", and $C_{T3}(h,M)$ for maximum "afterburner". "Idle" is defined as $0.1\cdot C_{T2}(h,m)$. In between the engine states C_T depends linearly on δ. Specific fuel consumption is given for "normal power", $C_{\dot{m}2}(h,M,\delta)$, and for "afterburner", $C_{\dot{m}3}(h,M,\delta)$. To have an analytical expression for the dependence on power setting we define

$$C_T = a\delta^2+b\delta+c \qquad (5)$$

where the coefficients a,b,c are determined from

$$\begin{aligned} C_T(h,M,0.1) &= C_{T1}(h,M) = 0.1\ C_{T2}(h,M) \\ C_T(h,M,1) &= C_{T2}(h,M) \\ C_T(h,M,2) &= C_{T3}(h,M) \end{aligned} \qquad (6)$$

resulting in

$$a = \frac{C_{T3}-2C_{T2}}{1.9}, \quad b = C_{T2}-1.1a, \quad c = 0.1a \quad . \qquad (7)$$

The aerodynamic coefficients are approximated using rational functions:

$$C_L = \sum_{i=1}^{nzcl} a_i \alpha^{nzcl-i} / \sum_{j=1}^{nncl} b_j \alpha^{nncl-j}$$

$$C_{DO} = \sum_{i=1}^{nzcd} a_i \alpha^{nzcd-i} / \sum_{j=1}^{nncd} b_j \alpha^{nncd-j} \qquad (8)$$

and a polynomial for C_{DK}:

$$C_{DK} = (a_1 \eta_K^2 + a_2 \eta_K)(M + a_3) \quad . \qquad (9)$$

The engine data are approximated with polynomials:

$$C_{Ti} = \sum_{j=1}^{ncth} \sum_{k=1}^{nctm} a_{jk} M^{nctm-k} h^{ncth-j}, \quad i=2,3$$

$$C_m = \sum_{j=1}^{ncmd} \sum_{j=1}^{ncmh} \sum_{k=1}^{ncmm} a_{ijk} M^{ncmm-k} h^{ncmh-j} \delta^{ncmd-i} \qquad (10)$$

The polynomial coefficients are determined by fitting the tabular data to the functions above which leads to the solution of a nonlinear least square problem for determining the coefficients in (8) and to the solution of a linear least square problem for the coefficients in (9) and (10).

Table 1: Number of polynomial coefficients

nzcl	nncl	nzcd	nncd
5	4	5	6
ncth	nctm		
5	3		
ncmd	ncmh	ncmm	
2	3	4	

Typical degrees of the approximating polynomials are given in Table 1. Figure 1 shows the graphs of (8) and the given data points. Figure 2 shows thrust coefficients and specific fuel consumption versus altitude and Machnumber for two engine states with linear interpolation between the data points. Accuracy of the approximation (10) is near 5% for specially selected range of the independent variables.

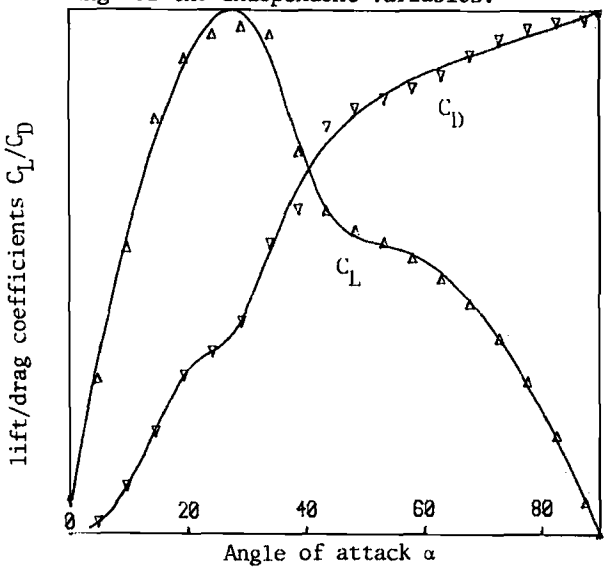

Fig. 1: Aerodynamic coefficients

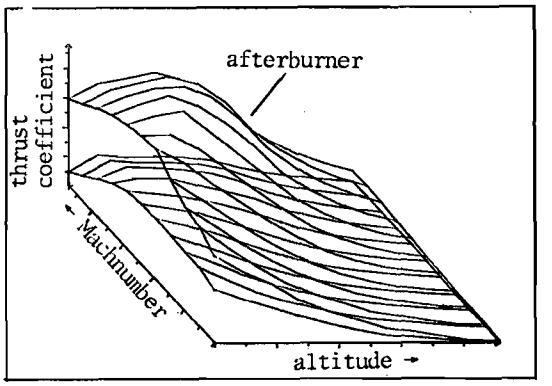

Fig. 2a: Thrust coefficents for normal power and afterburner

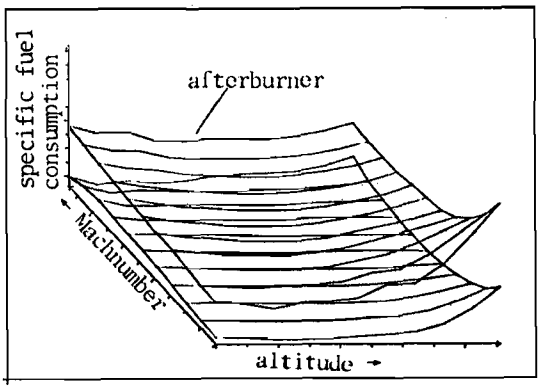

Fig. 2b: Specific fuel consumption for normal power and afterburner

Control Constraints

The control variables α, δ, and η_K are constrained by their minimum and maximum values. By introducing new control variables (subscript H) and with the relations

$$\begin{aligned} \alpha &= \alpha_{min} + (\alpha_{max} - \alpha_{min}) \sin^2 \alpha_H \\ \delta &= \delta_{min} + (\delta_{max} - \delta_{min}) \sin^2 \delta_H \\ \eta_K &= \eta_{Kmin} + (\eta_{Kmax} - \eta_{Kmin}) \sin^2 \eta_{KH} \end{aligned} \qquad (11)$$

the constraints are satisfied for all values of the auxiliary controls.

Constraint on Load Factor

The load factor is defined as

$$n = \begin{cases} n_{za} = (T_T \sin\alpha + L)/mg & \text{for conventional } \alpha \\ n_z = (L\cos\alpha + D\sin\alpha)/mg & \text{for Poststall} \end{cases} \qquad (12)$$

and constrained by its maximum value. n_z measures the acceleration in z-direction (body fixed reference axis) which the pilot must endure during Poststall maneuvers. n_{za} is the aerodynamic load factor. Both load factors have similar values for conventional flight. Numerically a violation of the load factor constraint is avoided by defining the additional differential equation and boundary conditions

$$\dot{\zeta} = \begin{cases} |n|-n_{max} & \text{if } |n|>n_{max} \\ 0 & \text{otherwise} \end{cases} \qquad (13)$$

$$\zeta(t_o) = \zeta(t_f) = 0 \quad .$$

Constraint on Pitch
For certain maneuvers it is required that

$$\theta(t) \geq 0 \qquad (14)$$

with

$$\sin\theta = \cos\alpha\sin\gamma+\sin\alpha\cos\mu\cos\gamma \quad . \qquad (15)$$

This constraint is handled the same way as the load factor constraint by adding the new differential equation and boundary equations

$$\dot{\kappa} = \begin{cases} \sin\theta & \text{if } \sin\theta<0 \\ 0 & \text{otherwise} \end{cases} \qquad (16)$$

$$\kappa(t_o) = \kappa(t_f) = 0 \quad .$$

Euler Angles

Besides velocity yaw angle χ, velocity pitch angle γ, velocity bank angle μ it is useful to have the yaw angle Ψ, the bank angle Φ, and the pitch angle θ. These angles are obtained by comparing coefficients of angular rotations from body axes to ground axes (subscript g) with those from body axes to wind axes to ground axes (see ref. [2]). The result is

$$\tan\Phi = \frac{\sin\mu\cos\gamma}{-\sin\alpha\sin\gamma+\cos\alpha\cos\mu\cos\gamma}$$

$$\tan\Psi = \frac{\cos\alpha\cos\gamma\sin\chi-\sin\alpha(\cos\mu\sin\gamma\sin\chi-\sin\mu\cos\chi)}{\cos\alpha\cos\gamma\cos\chi-\sin\alpha(\cos\mu\sin\gamma\cos\chi-\sin\mu\sin\chi)}. \qquad (17)$$

The expression for θ is given in (15). (17) is used to compute the aircraft attitude at any point along the trajectory for given control variables.

System Equations of Pursuer

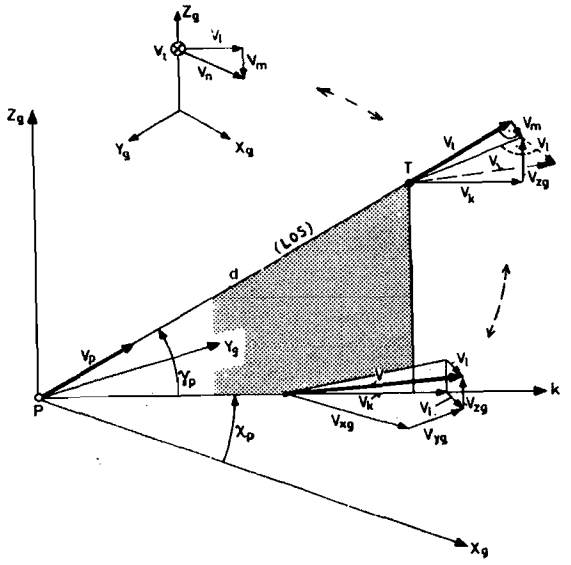

Fig. 3: Velocity components for equations of motion of pursuer

For the evasive maneuvers it is assumed that a pursuer (subscript P) follows aircraft A steering strictly according to a pure pursuit guidance law. With V_t: Velocity component along line of sight (LOS) (see Fig. 3), V_l: Velocity component perpendicular to the dotted vertical plane and to LOS, V_m: Velocity component parallel to vertical plane and perpendicular to LOS the equations of motion for the pursuer are

$$\begin{aligned} \dot{d} &= V_t-V_P \\ \dot{V}_P &= (T_P-D_P-m_Pg\sin\gamma_P)/m_P \\ \dot{\chi}_P &= -V_l/(d\cos\gamma_P) \\ \dot{\gamma}_P &= -V_m/d \\ \dot{x}_P &= V_P\cos\chi_P\cos\gamma_P \\ \dot{y}_P &= V_P\sin\chi_P\cos\gamma_P \\ \dot{h}_P &= V_P\sin\gamma_P \quad . \end{aligned} \qquad (18)$$

The velocity components described above are expressed in terms of the velocity components of aircraft A:

$$\begin{aligned} V_k &= V_{xg}\cos\chi_P+V_{yg}\sin\chi_P \\ V_l &= V_{xg}\sin\chi_P-V_{yg}\cos\chi_P \\ V_m &= V_k\sin\gamma_P-V_{zg}\cos\gamma_P \\ V_t &= V_k\cos\gamma_P+V_{zg}\sin\gamma_P \quad . \end{aligned} \qquad (19)$$

It is assumed that $m_P=m$, $T_P=T_{Pmax}$ and that the pursuer has the same aerodynamic and propulsive characteristics as aircraft A with the exception:

$$C_{AP} = C_{LP\alpha}\alpha_P \leq C_{LPmax} \qquad (20)$$

where $C_{LP\alpha}$ is approximated by some constant.

Since $\dot{\chi}_P$ and $\dot{\gamma}_P$ are determined by the trajectory of aircraft A α_P and μ_P could be obtained from (18-2) and (18-3) by solving the two equations iteratively. However, it is not necessary to know μ_P, only α_P is required, which is computed approximately via the resulting angular velocity ω_P of LOS:

$$\omega_P = \sqrt{\dot{\chi}_P^2\cos^2\gamma_P+\dot{\gamma}_P^2} = V_n/d \qquad (21)$$

and the resulting normalized acceleration n_P:

$$n_P = \omega_P\cdot\frac{V_P}{g} = \frac{V_nV_P}{gd} \quad . \qquad (22)$$

Then α_P is:

$$\alpha_P = \frac{n_Pm_Pg}{C_{LP\alpha}\frac{\rho_P}{2}SV_P^2+T_P} \qquad (23)$$

and the differential equations (18) can be integrated once some given initial state of the pursuer has been specified. The aspect angle β of the velocity vectors of aircraft A and the pursuer is computed from the inner product as

$$\cos\beta = \cos\gamma\cos\gamma_P\cos(\chi-\chi_P)+\sin\gamma\sin\gamma_P \quad . \qquad (24)$$

β is important for the interpretation of the results obtained.

Optimal Control Problem and Numerical Methods

Optimal Control Problem (OCP)

The OCP of the previous section consists of finding the control functions $\alpha_{II}(t),\mu(t),\delta_{II}(t),\eta_{KII}(t)$ for the differential systems (1), (13-1), (16-1), and (18) subject to boundary conditions that will be specified in the next section. The system is to be controled such that the final state is reached in minimum time. With x: state vector, u: control vector, φ: vector of right hand sides the OCP at hand is stated as:

$$\text{minimize } \Phi(x,\pi)_1 \tag{25}$$

subject to

$$\dot{x} = \varphi(x,u,\pi), \quad 0 \le t \le 1 \tag{26}$$

$$x(0) = \text{given}, \quad \Psi(x,\pi)_1 = 0 \quad . \tag{27}$$

It is assumed that the independent variable time t has been normalized, the parameter π (a scalar) represents the free final time t_f. Necessary conditions for optimality are:

$$\dot{\lambda} = H_x, \quad H_u = 0, \quad 0 \le t \le 1 \tag{28}$$

$$(H_\pi)_1+\Phi_\pi+\Psi_\pi\nu = 0 \tag{29}$$

$$\lambda+\Phi_x+\Psi_x\nu = 0 \tag{30}$$

where $\lambda(t)$ and ν are Lagrange multipliers and the Hamiltonian $H = -\lambda^T\varphi$.

Numerical Solution of OCP

The most common numerical technique for solving an OCP is to parametrize the control function and solve the resulting nonlinear programming problem (NLP) using one of the many NLP-solvers available (see references [3]-[5]). The method used in this paper is described in more detail in [5]. It consists of selecting a grid t_i, i=1,...,n_g, using the values of the control functions at the grid points $u(t_i)$ as parameters of the problem, and interpolating in between using cubic spline functions. The resulting NLP consists of finding the components of the decision vector

$$y = (u_1(t_1),u_1(t_2),\ldots,u_m(t_{ng}),\pi)^T \tag{31}$$

such that

$$c_j(y) = \Psi_j(x,\pi)_1, \quad j=1,\ldots,q \tag{32}$$

and also

$$f(y) = \Phi(x,\pi)_1 \tag{33}$$

is minimized subject to the appropriate differential system and initial conditions. The above problem is converted into an unconstrained problem by minimizing the Lagrangian

$$L(y,\vartheta,\sigma) = f(y)+\tfrac{1}{2}(c-\vartheta)^T\sigma(c-\vartheta) \tag{34}$$

where σ is a diagonal qxq matrix of penalty constants and ϑ a q-vector of an outer iteration loop. The NLP algorithm consists of the following steps:

i) select y^0,ϑ^1,σ^1

ii) $k = k+1$
$y^k = \arg\min_y L(y,\vartheta^k,\sigma^k)$

iii) if $\|c^k\| < \|c^{k-1}\|\cdot\rho, \quad 0 < \rho < 1$
then $\vartheta^{k+1} = \vartheta^k-c(y^k)$
$\sigma^{k+1} = \sigma^k$
otherwise $\vartheta^{k+1} = \vartheta^k$
$\sigma^{k+1} = \eta\sigma^k, \quad \eta > 1$

iv) if $\|c^k\| < \varepsilon_1$ and $\|L_y^k\| \le \varepsilon_2$ stop
otherwise go to ii).

The differential system is always satisfied by using a Runge-Kutta 7/8th order initial value solver. In minimizing L partial derivatives with respect to y are needed. In this paper they are computed using impulsive response functions as suggested in [4].*

Minimum Time Maneuvers

Turning Maneuvers

All turning maneuvers are characterized by boundary conditions

$$V_o,\ \chi_o = 0,\ \gamma_o = 0,\ h_o,\ x_{g_o},\ y_{g_o}$$
$$\chi_f = 180^o,\ \gamma_f = 0 \quad . \tag{34}$$

Free turning has no additional boundary conditions, final velocity and altitude are selected optimally. Figures 4 and 5 show trajectories and control actions for V_o=100 and 300 m/s. Figure 6 depicts the maneuvers in a $|\dot{\gamma}|_{max}$-V diagram.

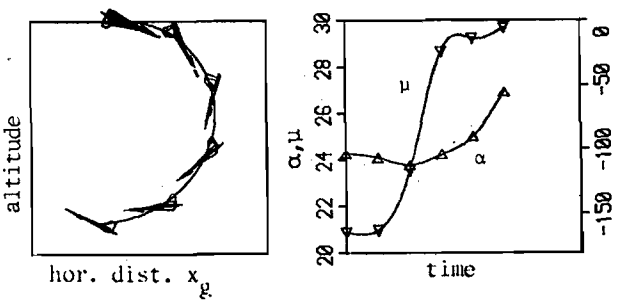

Fig. 4: Free turning maneuver (V_o = 100 m/s)

*The work of D. Kraft is acknowledged here who generated and tested a general code for the algorithm which is described in the proceedings of the first IFAC Workshop on Control Applications of Nonlinear Programming, Denver, 1979.

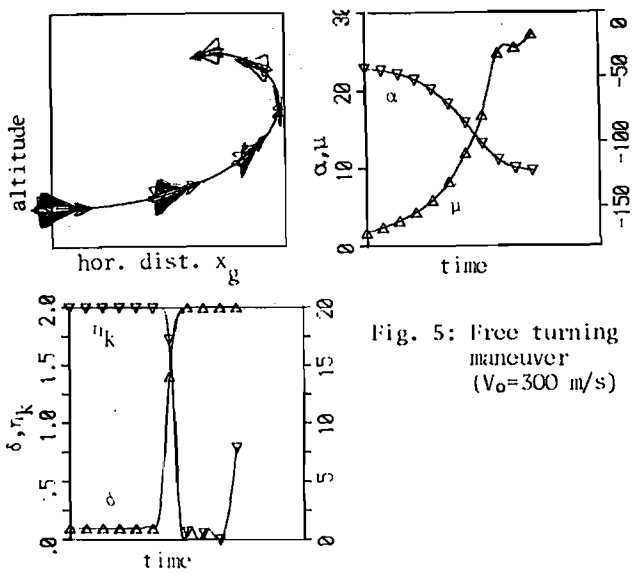

Fig. 5: Free turning maneuver (V_o=300 m/s)

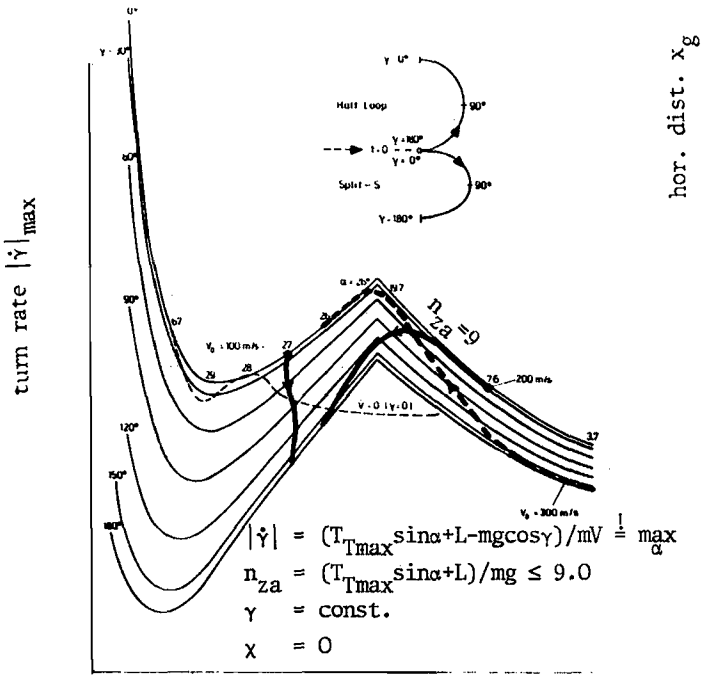

Fig. 6: Free turning maneuvers in $|\dot{\gamma}|_{max}$ (V,γ) diagramm

The diagram is valid for flight in the vertical plane (half loop or split-S) and shows maximum instantaneous "turn rates" $|\dot{\gamma}|$ as function of velocity and path inclination subject to a load factor constraint. The highest "turn rate" outside the poststall region is achieved at $V=V_C$, V_C being the corner velocity. Inside the poststall region extremely high turn rates can be achieved. During a half loop (from $\gamma=180°\rightarrow0°$) -executed at constant speed - "turn rates" increase, during a split-S ($\gamma=0°\rightarrow180°$) turn rates decrease due to the gravitational acceleration. Depicted also is the maximum turn rate for $\dot{V}=0$. The diagram shows the sequence of states for the optimal maneuvers. For V_o=100 m/s the optimal maneuver is a split-S flown at nearly constant velocity. In contrast to an exactly constant speed maneuver (m) the angle of attack is in the beginning less 27° in order not to decelerate too much - resulting in a decreased turn rate. Only at the end of the maneuver is α=27° (best instantaneous turn rate) achieved (see also Fig. 4). For V_o=200 m/s the m. starts at the aerodynamic load limit. In order to fly at high turn rates velocity is initially decreased (δ=0.1, $\eta_K=\eta_{Kmax}$). Just before reaching the corner veloxity, however, δ=2 and η_K=0 is optimal control action. For V_o=300 m/s the optimal m. tends toward a half-loop. Here, the gravitational force assists the deceleration process necessary in order to fly near the corner velocity. Thrust and speed brakes are used in a similar sequence as for V_o=200 m/s. Since the trajecotry is not exactly in the vertical plane the m. has only a dotted line since Fig. 6 applies to flight in the vertical plane only.

A turning maneuver with prescribed final altitude is shown in Figure 7. The m. is flown mainly in the horizontal plane with α near C_{Lmax}. Figure 8 shows various m. in the $\dot{\chi}$-V diagram.

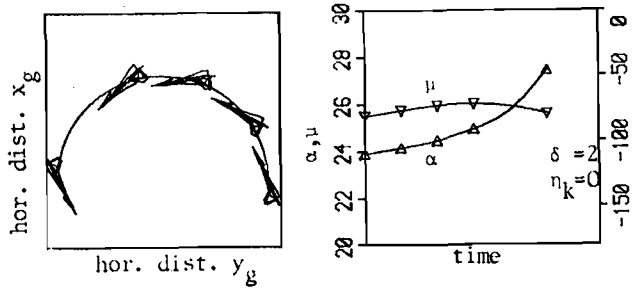

Fig. 7: Turning maneuver with final altitude prescribed (V_o=100 m/s)

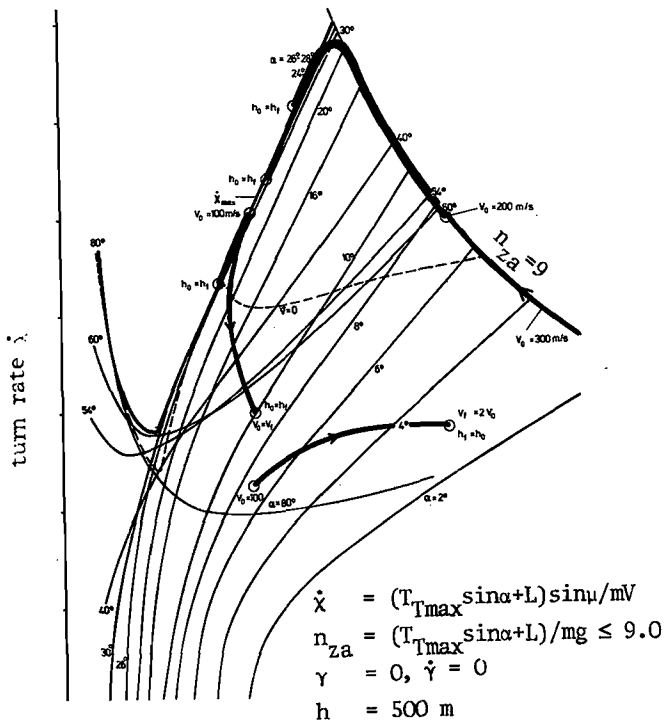

Fig. 8: Turning maneuvers in $\dot{\chi}(V)$ diagram

The diagram illustrates instantaneous turn rates in the horizontal plane subject to the load factor constraint. The highest turn rates again are achieved at $V=V_C$ and in the poststall region. Also shown is the turn rate for $\dot{V}=0$. For $V_o=100$ m/s the optimal m. is flown along the $\dot{\chi}_{max}$ boundary, final velocity being somewhat smaller than V_o. For $V_o=200$ m/s the m. begins at the load limit boundary, throttle setting and speed brakes are used in the same way as for the m. in the vertical plane. The m. ends at a smaller velocity than V_C on the $\dot{\chi}_{max}$ boundary and for the m. with $V_o=300$ m/s control actions and the sequence of states are very similar. Depicted, in addition, is a m. with *final altitude and velocity prescribed*. Here, the high angle of attack time history of the corresponding m. with free final velocity and fixed final altitude is modified such that at the end α is decreased to about 10°. For $V_f=2*V_o$ angle of attack time history varies from about 7° to 3°.

Control time histories and trajectories of aircrafts A and B with $\alpha_{max}=90°$ and 30°, respectively, where *final velocity, altitude and path coordinates are prescribed* are shown in Figure 9.

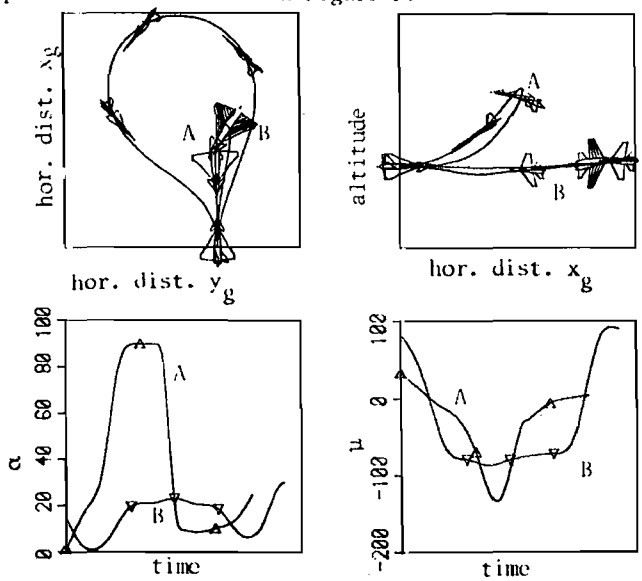

Fig. 9: Turning maneuvers with final altitude, velocity, path coordinates prescribed (V_o= 100 m/s, $h_o=h_f$, $x_{go}=x_{gf}$, $y_{go}=y_{gf}$, striped wing area indicates: aircraft viewed from bottom)

A has a time advantage over B of 19%. The optimal m. for A consists of a pull up m., a roll from head down to head up position, and a return to the initial position. The optimal m. for B consists of a turn to the right, to the left, and at the end to the right again. The m. for A is executed mainly in the vertical plane while B flies mainly in the horizontal plane. Besides time advantages A also needs less "space" for the maneuver.

Pointing Maneuver

This maneuver shows the pointing capability of A. It is assumed that two aircraft pass each other at time t_o in opposite direction at x_{go},y_{go},h_o (see Figure 10). Aircraft E (evader) continues flying in $(-x_g)$-direction with constant speed V_E ($\dot{x}_E(t)=-V_E$, $y_E(t)$=const., $h_E(t)$=const.). Aircraft A - the pursuer - is to point the fuselage in minimum time towards E. The corresponding boundary conditions are:

$$\begin{aligned} \cos\Psi_f+(x_{gf}-x_E(t_f))/\tau_H &= 0 \ , \\ \sin\Psi_f+(y_{gf}-y_{go})/r_H &= 0 \ , \\ \cos\Theta_f-r_H/\tau_V &= 0 \ , \\ \sin\Theta_f+(h_f-h_o)/r_V &= 0 \ , \end{aligned} \qquad (35)$$

with $r_V=\sqrt{r_H^2+(h_f-h_o)^2}$ and Θ, Ψ from (15) and (17-2). Figure 10 shows the control time histories and the trajectory in the horizontal plane. For $V_o=100$ m/s the maneuver consists of a turn with α near $C_{L_{max}}$ followed by a sudden pointing action of the aircraft towards E. For $V_o>100$ m/s the maneuver sequences are similar.

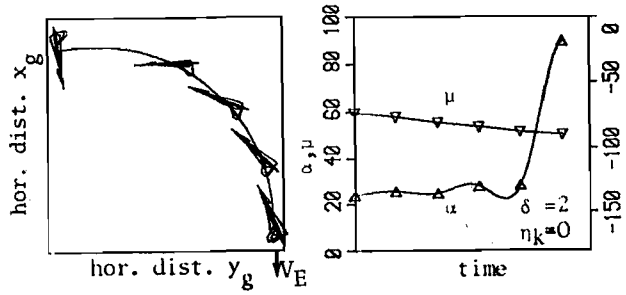

Fig. 10: Pointing maneuver (V_o=100 m/s)

Slicing Maneuver

The slicing maneuver consists of two turning maneuvers in opposite direction. The first part is characterized by the initial conditions

$$V_o = 100 \text{ m/s}, \ \chi_o = \gamma_o = 0, \ x_{go}, \ y_{go}, \ h_o. \qquad (36)$$

Final conditions for the first part are

$$\chi_{1f} = 180°, \ \alpha(t_{1f}) = \alpha_{max} \ . \qquad (37)$$

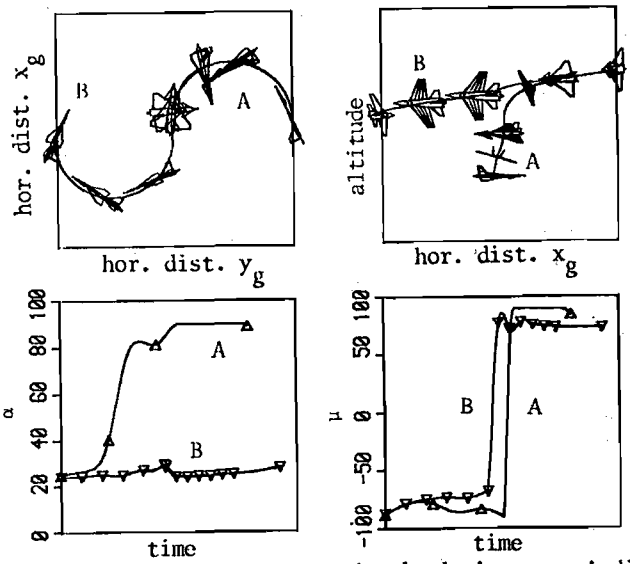

Fig. 11: Slicing maneuver (striped wing area indicates: aircraft viewed from bottom)

Initial conditions for the second part are identical to the final conditions of the first part. Final condition for the second part is:

$$\chi_{2f} = 0^{\circ} \qquad (38)$$

During the second part of the maneuver $\theta \geq 0$ is required. Figure 11 shows control time histories for aircrafts A and B and the trajectories. While B flies two turn at α near C_{Lmax}, aircraft A makes a typical PST-maneuver in the second part consisting of a stationary steep descent with high turn rates about the velocity vector and $\theta \approx 0$.

The time advantage of A compared with B is 15%. If instead of (37) and (38) fuselage direction would have been chosen as boundary conditions time advantages would have been even greater (approximately 50%). The high yaw required for the optimal PST turn (second part), however, can not be achieved in practice and therefore the maneuver will be slower altogether.

Evasive Maneuvers

At the beginning of the maneuvers both aircraft A and the pursuer (index P) are flying at the same altitude. P has visual contact and flies either perpendicular or parallel to A. Initial conditions are defined by:

$$\chi_o, \chi_{P_o}, \gamma_o, \gamma_{P_o}, V_o, V_{P_o}, h_o, h_{P_o}, d_o \quad . \qquad (39)$$

Final condition

$$n_{Pf} = n_{max} \qquad (40)$$

guarantees that the pursuer overshoots his target. For $V_o = V_{P_o} = 130$ m/s and $\chi_o - \chi_{P_o} = 90^{\circ}$ Figure 12 shows optimal control time history and the trajectory in the horizontal plane.

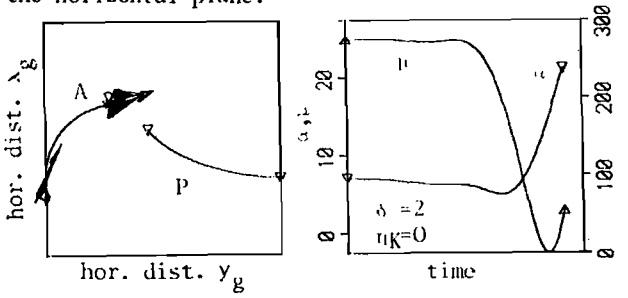

Fig. 12: Evasive maneuver with pursuer coming from the side ($\chi_o - \chi_{P_o} = 90^{\circ}$)

The optimal evasive maneuver consists of a turn essentially in the horizontal plane with α near C_{Lmax}. It ends with a sudden change in bank angle in opposite direction and with small angle of attack resulting in an acceleration in order to achieve a high velocity component V_n (see eq. 22), the final aspect ratio β being approximately 90°. Again the high roll rates can not be achieved in practice, but the character of the maneuver will remain the same even if limitations are enforced.

For the same initial velocities but $\chi_o - \chi_{P_o} = 0$, i.e. the pursuer coming from behind, the optimal evasive maneuver is shown in Figure 13. It consists essentially of a split-S followed by an acceleration phase with small angle of attack. At the end of the maneuver A again tries to fly perpendicular to LOS by changing the bank angle by 180°, final aspect angle β being near 90° too.

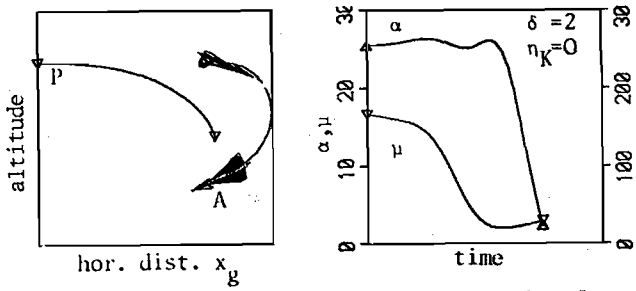

Fig. 13: Evasive maneuver with pursuer coming from behind ($\chi_o - \chi_{P_o} = 0^{\circ}$)

Summary and Conclusions

Several aircraft maneuvers have been investigated in order to find out if the Poststall-capability of a future tactical fighter improves performance. All maneuvers have in common that either flight path heading or fuselage heading are to be changed in minimum time. Load factor constraints and constraints on aircraft attitude as well as requirements on final velocity, altitude, path coordinates, load factor of the pursuing aircraft, and angle of attack characterize the maneuvers in detail. The simplifying principle that governs all optimal control actions is the tendency to fly at maximum instantaneous turn rate ($\dot{\chi}_{max}, |\dot{\gamma}|_{max}$) as long as requirements on final velocity do not correspond with smaller angles of attack. For sufficiently large initial velocities power setting and speed brakes are used such that flight occures near the corner velocity (intersection of C_{Lmax} and n_{Zamax}-boundaries) as much as possible because instantaneous turn rates are the highest there. Deceleration into the Poststall region - where instantaneous turn rates become very large - and subsequent acceleration to the required final velocity has only been observed for one special TM (fixed final state) for sufficiently small initial velocities. For the SM - which is a typical poststall maneuver - poststall has time advantages. because of the extremely large turn rates.

In addition to time advantages due to PST there are other advantages such as the pointing capability and the capability of maneuvering in a small area. Further investigations should include constraints on maximum pitch- and roll rates.

References

[1] K.H. Well, B. Faber, E. Berger (1979) Optimale taktische Flugmanöver für ein Kampfflugzeug der 90er Jahre, DFVLR A552-79/6.

[2] A. Miele (1962) Flight mechanics I, theory of flight paths, Addison-Wesley, Reading, Mass.

[3] D.G. Hull (1974) Application of parameter optimization methods to trajectory optimization, AIAA Mechanics and Control of Flight Conference, Anaheim.

[4] R.G. Brusch, J.P. Peltier (1973) Parametric control models and gradient generation by impulsive response, 24. IAF Congress, Baku.

[5] P.E. Gill, W. Murray (1974) Numerical methods for optimization, Academic Press.